Article:
Fang, L, Wang, P, Zeng, Q et al. (5 more authors) (2019) Measurement of interphase forces based on dual-modality ERT/DP sensor in horizontal two-phase flow gas-water. Measurement, 136. pp. 703-717. ISSN 0263-2241

https://doi.org/10.1016/j.measurement.2018.12.104

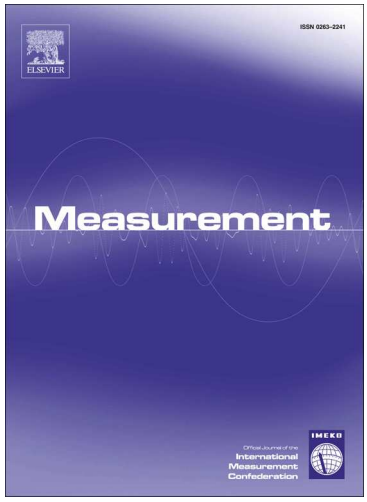

Measurement of Interphase Forces based on Dual-modality ERT/DP Sensor in Horizontal Two-phase Flow Gas-water

Lide Fang, Peipei Wang, Qiaoqiao Zeng, Mingming Li, Xiaoting Li, Mi Wang, Yousef Faraj, Qiang Wang

PII: S0263-2241(18)31249-1
DOI: https://doi.org/10.1016/j.measurement.2018.12.104
Reference: MEASUR 6238

To appear in: *Measurement*

Received Date: 2 May 2018
Revised Date: 13 December 2018
Accepted Date: 30 December 2018

Please cite this article as: L. Fang, P. Wang, Q. Zeng, M. Li, X. Li, M. Wang, Y. Faraj, Q. Wang, Measurement of Interphase Forces based on Dual-modality ERT/DP Sensor in Horizontal Two-phase Flow Gas-water, *Measurement* (2018), doi: https://doi.org/10.1016/j.measurement.2018.12.104

Measurement of Interphase Forces based on Dual-modality ERT/DP Sensor in Horizontal Two-phase Flow Gas-water

Lide Fang[a,b,c], Peipei Wang[a,b,c], Qiaoqiao Zeng[a,b,c], Mingming Li[a,b,c], Xiaoting Li[a,b,c], Mi Wang[d], Yousef Faraj[e], Qiang Wang[d]

[a]College of Quality & Technical Supervision, Hebei University, Baoding, Hebei, 071002, China
[b]Measuring Instruments and Systems Engineering Laboratory of Hebei Province,Baoding 071000,Hebei,China
[c]The Research Center of Industrial Metrology Engineering Technology of Baoding,Baoding 071000,Hebei,China
[d]Faculty of Engineering, University of Leeds, Leeds, LS2 9JT, UK
[e]School of Chemical of Engineering, Sichuan University, Chengdu, Sichuan 610065, PR China

Abstract

In order to better understand the mechanisms of two-phase flow and the prevailing flow regimes in horizontal pipelines, the evaluation of interphase forces is paramount. This study develops a method to quantitatively estimate the interphase force in two-phase gas-water flow in horizontal pipeline. The electrical resistance tomography technology is used to measure the void fraction, while the differential pressure perpendicular to the horizontal pipe is measured in different flow patterns via a Differential Pressure sensor. The inner pipe diameter is 50 mm, the water flow range from 3.26 m^3/h to 7.36 m^3/h, the gas flow rate range from 1 to 60 l/min, which covered a range of flow patterns, the absolute pressure range from 0.07 MPa to 0.12 MPa. The relationship between the differential pressure drop and interphase force is established, and the effects of these forces on the flow are analyzed. Experimental results indicate that the dual-modality measurement system was successfully provided a quantitative evaluation of interphase forces in two-phase horizontal gas-water flow.

Keyword: Interphase forces; Gas-liquid two-phase flow; Horizontal flow; Void fraction; Differential pressure

1. Introduction

The substances in nature are divided into three types: gas phase, liquid phase and solid phase. Single-phase flow is the flow of single-phase material, multiphase flow is a complex phenomenon involving simultaneous flow of two or more physically immiscible fluids (such as: oil and water) in pipelines. The study of highly viscous multiphase flow systems is fundamental to the oil industry. In heavy oil production fields, the transport of production fluids, i.e., oil, water and gas, commonly occurs as a "foamed emulsion" flow (i.e., a water-in-oil emulsion with dispersed gas flowing as a foam) [1-2]. Oil-water and gas-water two-phase flows are often encountered in petroleum, chemical and petrochemical industries [3-5]. Due to the complex interface, a series of interface problems have not been solved so far, they are still the key to gas-liquid flow research, including phase distribution mode, inter-phase mechanism and microscopic turbulence structure. A complete description of the phase interaction mechanism should take into account the interphase forces. The interphase forces play a crucial role in the gas-liquid two-phase flow model as they constitute a mechanical balance between the phases and determine the phase distribution pattern across the flow channels. Many of important design and engineering parameters such as pressure drop, mass transfer, heat transfer etc, are closely related to the interphase force [6]. It is divided into three parts: drag, the lateral force (lift) and additional mass force [7-8]. In order to describe the flow and the interaction between the constituent phases, experimental analysis of the flow has to be carried out first, then it can be followed by establishing a theoretical explanation [9]. The magnitude of interphase forces can be reflected by pressure or differential pressure signals. The traditional method to measure the pressure drop along the flow direction cannot provide a

direct measurement of the interphase force, as it is associated with the frictional pressure drop and the acceleration pressure drop, as a result it is difficult to distinguish. The researchers therefore always ignore the quantitatification of interphase force or just carry out a simple analysis.

The aspects of interphase force in multiphase flow and other fields have been touched upon by several researchers. Wang et al. [10] analyzed different correlations for the interphase forces including the drag, lift, wall lubrication, and turbulent dispersion force, and systematically investigated their predictive features. Gadiraju et al. [11] reported exact solutions for fully developed, steady, laminar flow of a particle fluid suspension in a vertical circular pipe, The solutions were based on a typical finite volume fraction two phase flow model of the continuum type. It is pointed out that the lift force contribution to interphase force can't be expressed in closed form. Tabib et al. [12] studied the interphase force through CFD simulation, in which they have presented 3D transient CFD simulation of bubble column for a wide range of superficial gas velocity on a relevant industrial cylindrical column. Li et al. [13] investigated the relative importance of interphase forces and their effect on particle transverse motion in a particle-laden channel turbulence. In other fields, Rybaczek et al. [14] demonstrate the existence of constitutive (interphase and mitotic) Chk1 kinase phosphorylation, the translocation of its phosphorylated form from the nucleus to cytoplasm in prometaphase as well as strong labeling of apoptotic nuclei with alpha-Chk1(S317) antibodies. Riaño et al. [15] studied the influence of interphase region on composites based a FEA homogenization technique. However, these studies in two-phase flows have not provided an experimental verification regarding interphase force in horizontal two-phase gas-water flows.

There are two main types of intelligence that are artificial intelligence [16] and machine intelligence [17]. In electronic systems, mainly machine intelligence is used. Machine vision is a non-destructive grading technology and cost-effective method with high accuracy that has a variety of branches, and it is very useful for measuring the interphase forces. One of these branches is radar-based machine vision systems. Radar signal recognition is of great importance in the field of electronic intelligence reconnaissance. It has extensive research in various fields. To deal with the problem of parameter complexity and agility of multi-function radars in radar signal recognition. SAR imaging systems are known as the most popular remote sensing technique greatly used in the past decades because of its good performance in extreme weather scene imaging [18]. It provides an effective way to image all day and all weather, which is incomparable by other sensors. In order to recognize and identify selected objects, SAR can provide high-resolution images to distinguish terrain features. Various tasks of SAR images have been found, such as segmentation [19], classification [18], target recognition [20], change detection [21], or a combination of them [22]. Alzeyadi et al. [23] applied the synthetic aperture radar (SAR) imaging and the K-R-I (curvature-area-amplitude) transform to measure moisture in a concrete panel specimen (water-to-cement ratio = 0.45). Akbarizadeh et al. [24] have worked hard to integrate spectral clustering and Gabor feature clustering, leading to improved segmentation results of SAR images. Karimi et al. [25] evaluated on two pairs of real radar and optical sentinels and advanced land observation satellite (ALOS) images, and evaluated the impact of RS-LDASR(a new algorithm based on the combination of random subspace (RS), linear discriminant analysis and sparse regularization (LDASR)) on classification results in dimension reduction and supervisory feature selection and learning.

The differential pressure fluctuation signal contains information many parameter information in the two-phase flow system. The measurement of two-phase flow by differential pressure has always been a research topic in the fields of power, chemical engineering and nuclear power engineering. Differential pressure sensors are widely used in many high-precision measurement applications such as micro-flow measurement, leak test, clean room monitoring, environmental sealing test, gas flow measurement, and

liquid level measurement. The disadvantage is that when used in two-phase flow, the instability of the differential pressure signal is increased due to the certain disturbance generated by the fluid itself. Venugopal et al. [26] studied the sensitivity of the dynamic differential pressure sensor, which provided a basis for the application of vortex flowmeter. Wang et al. [27] proposed a novel flow measurement method for gas-liquid two-phase slug flow by using the blind source separation technique. The flow measurement model is established based on the fluctuation characteristics of differential pressure (DP) signals measured from a Venturi meter. Zhang et al. [28] analyzed the influence of mass flowrate, pressure, voidage and density on DP signals, and provided the relationship between voidage of gas-liquid two-phase flow and root-mean-square deviation of the DP fluctuating signals measured from a Venturi meter. Some multiphase flow meters are based on differential pressure measurement across obstructions, including orifice plates [29] and Venturi tubes [30].

The void fraction detection technology and method mainly include Quick Closing Valve, ray absorption method, electrical method and optical method [31]. The Quick Closing Valve is reliable and effective, but it cannot implement online real-time measurement [32]. Ray absorption method is costly and has a great safety risk. The electrical method can no longer meet the needs of online measurement [33]. The optical method has a simple structure and has a good effect on the measurement of the two-phase flow rate. However, there is a certain requirement on the cleanliness of the measured medium [34]. Electrical resistance tomography technology (ERT) is formed and developed in 1980s, which belongs to a kind of Process Tomography (PT technology, it's the product of the combination of computer application technology and modern detection technology, and it's the two-phase flow/ multiphase flow measurement technology developed in recent years). ERT is provides useful information of flow characteristics, including gas/solid, gas/liquid and liquid/liquid, as an on-line measuring technique possessing the advantages of visualisation, low-cost, non-invasion and robustness, it has become an accepted measuring technique in process applications. The disadvantage is that the measurement range is limited. Yunus et al. [35] developed a three-dimensional (3D) and two-dimensional (2D) ultrasonic transmission/ electrical resistance tomography (UT/ERT) model using the finite element method (FEM) with COMSOL software for imaging two-phase gas/liquid. Annamalai et al. [36] studied the two-phase flow homogeneity downstream of a slotted orifice by an ERT system. Adetunji et al. [37] used ERT coupled to Dynamic Gas Disengagement for the estimation of bubble rise velocities and bubble population sizes in a column.

Pressure fluctuations are sensitive and can be easily influenced by many factors. Many previous studies only mentioned the interphase force in the study of pressure drop, and usually ignored the phase interaction or only qualitative analysis. The innovation of this study is to study the physical model and mathematical model of the interphase force, and make the use of differential pressure signal, based on the gravity differential pressure fluctuation signal perpendicular to the horizontal pipe, it is perpendicular to the flow direction, thus it is not affected by the resistance along the way. It is worth mentioning that this method avoids the measurement error caused by the joining pipe in the traditional differential pressure measurement, and avoids the shortcomings of coupling of the interphase forces with the frictional pressure drop and the acceleration pressure drop. At same time proposed a method for obtaining phase holdup and can reflect the interaction between the constituent phases (gas-liquid). The gas-liquid two-phase flow detection device was designed to realize the quantitative detection estimate the interphase force, and finally achieved the effect of improving of the qualitative analysis of the interphase force in the previous research. In order to achieve the above objective, three main tasks have to be carried out: First, establishing the relationship between the gravity pressure drop and interphase force; Second, designing an

experimental system to test the gravity pressure; Third, obtaining the interphase forces of different flow modes and velocities.

2. Theoretical analysis

Some studies have provided suitable distribution models for the target in various fields. For example in the SAR field [38-39], in the task [40-41] was attempted to segment SAR images in two phases by applying the curvelet coefficient energy and an unsupervised spectral regression method and proposed a new parameter estimation technique (KCE) to describe SAR image segmentation, it with fewer coefficients than KWE. This proposed algorithm performed better than the other algorithms. G. Akbarizadeh et al [38] proposed a curvelet and watershed-based method for segmentation of SAR images and recognition of various textures in them, and curvelet is an effective method for noise reduction and extracting useful features. And Farbod et al. [42] proposed an optimized fuzzy cellular automata algorithm for SAR image edge detection. Fang et al. [43] detected flow noise of gas-liquid two-phase flow in horizontal pipeline by using the acoustic emission technique, and processed signals by wavelet transform and chaotic analysis. Eishita et al. [44] employed two noise models: a unimodal zero mean Gaussian noise model-a canonical model in sensor systems, and a multimodal noise process generated from a sequential noise model. The final outcomes provided guidance for the AR game development community and other researchers in this arena. The model of this paper is established as follows:

Based on previous studies, the interphase forces of gas-liquid two phase flow can be divided two types: the first type is the force which is perpendicular to the flow direction, the second is the force which is parallel to the flow direction. Previous studies have used modern spectral analysis, neural networks and intelligent computing, nonlinear system dynamics, and so on. The emphasis is placed on the analysis of the laws between the experimental phenomena and the measured signals, however, an in-depth insight of the interaction between gas-liquid two-phase forces contained in the fluctuation signals has not been reported [45].

The Darcy friction factor is a dimensionless expression, making it easier to use and draw comparisons between different flows [46].

$$h_f = \frac{\Delta P_f}{\rho} = 2\,f\,\frac{u^2 l}{d} \tag{1}$$

$$\lambda = 4\,f \tag{2}$$

Where h_f is resistance loss, f is adimensionless cofficient called thedarcy friction factor, λ is the friction coefficient, d is the pipe diameter, l is the pipe length, ρ is density and u is average flow velocity.

Flow resistance in the horizontal pipeline can be divided into two types: resistance along the pipeline and local resistance in the tube [47]. Using the above Eqs. (Eq. (1) and Eq. (2)), the resistance along the pipe way for the steady flow in the pipe can be obtained by the Eq. (3):

$$\Delta P_f = \rho h_f = \lambda \frac{l}{d} \cdot \frac{\rho u^2}{2} \tag{3}$$

If we assume that l=0, then the resulting $\Delta P_f = 0$, which is an indication of non-viscous flow (i.e. the shear stress acting on the fluid within the pipe is zero and there no friction in the same section of the pipeline). Therefore, the gravity pressure drop is the pressure difference measured in the vertical position of horizontal direction, which is unaffected by friction resistance. As shown in Fig. 1, the differential pressure of AC is the pressure drop resistance along the pipe way, the differential pressure of AB is the

differential pressure across the pipe cross-sectional area, and it is not affected by the resistance along the pipe, and it is the gravity pressure drop.

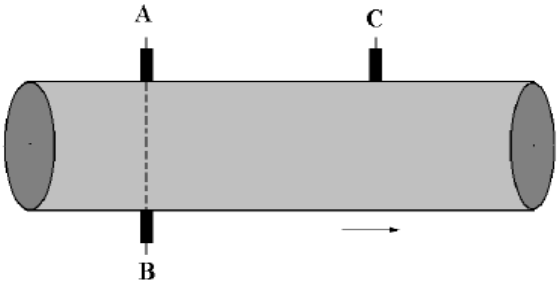

Fig. 1. Pressure difference in horizontal pipeline.

Consider single-phase irrotational flow conditions, Navier - stokes equations can be shown in the Eq. (4):

$$\left.\begin{aligned} f_x - \frac{1}{\rho}\frac{\partial P}{\partial x} + \upsilon\nabla^2 v_x &= \frac{\partial v_x}{\partial t} + v_x\frac{\partial v_x}{\partial x} + v_y\frac{\partial v_x}{\partial y} + v_z\frac{\partial v_x}{\partial z} \\ f_y - \frac{1}{\rho}\frac{\partial P}{\partial y} + \upsilon\nabla^2 v_y &= \frac{\partial v_y}{\partial t} + v_x\frac{\partial v_y}{\partial x} + v_y\frac{\partial v_y}{\partial y} + v_z\frac{\partial v_y}{\partial z} \\ f_z - \frac{1}{\rho}\frac{\partial P}{\partial z} + \upsilon\nabla^2 v_z &= \frac{\partial v_z}{\partial t} + v_x\frac{\partial v_z}{\partial x} + v_y\frac{\partial v_z}{\partial y} + v_z\frac{\partial v_z}{\partial z} \end{aligned}\right\} \quad (4)$$

The mass force refers to the external forces acting on fluid particles, it is usually the force of the fluid mass. Where, f_x, f_y, f_z is the mass force of the three coordinate directions, v_x, v_y, v_z is the velocity of the three coordinate directions, v is the kinematic viscosity, P is the pressure.

Assuming that the flow cross-section of the pipeline is constant and coincident with the flowing section, because there is no velocity component in the flowing section, let the axial direction of the pipe(x direction) vertical to the flowing section, the Navier-stokes equations of the X-axis and Y-axis direction can be shown in Eq. (5):

$$\left.\begin{aligned} f_y - \frac{1}{\rho}\frac{\partial P}{\partial y} &= 0 \\ f_z - \frac{1}{\rho}\frac{\partial P}{\partial z} &= 0 \end{aligned}\right\} \quad (5)$$

This shows that the fluid pressure in the cross-section should be consistent with the pressure distribution law of fluid statics:

$$z + \frac{P}{\rho g} = C \quad (6)$$

Where Z is the fluid position potential energy, C is the integral constant.

As shown in Fig. 2, setting the bottom of the pipe as the equipotential surface, $z_1=0$, then:

$$\frac{P_1}{\rho g} = z_2 + \frac{P_2}{\rho g} \quad (7)$$

$$P_1 - P_2 = z_2\rho \quad (8)$$

Eq. (8) shows that the differential pressure in the vertical direction of non rotating single phase flow in horizontal pipe is the gravity pressure drop.

There are many kinds of flow patterns of gas-liquid two-phase in horizontal pipe, it is worth mentioning that the stratified flow is the most simple and intuitive flow pattern in the analysis of the two-phase flow under the horizontal adiabatic flow. Here stratified flow pattern is used for analysis in this paper. Assuming that the two phase is completely separated, the sum of flow section of gas-liquid two phase flow equals the total cross section of the flow channel, as shown in Fig. 3.

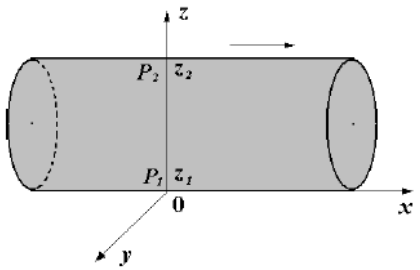

Fig. 2. Single phase of horizontal pipe flow diagram.

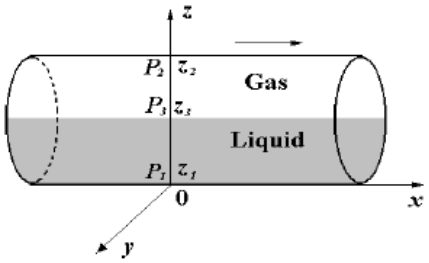

Fig. 3. Gas liquid two phase flow diagram.

Regardless of the interaction between the two phases, the flow characteristics of each phase in the two-phase flow can be analyzed separately by the basic equation of the single phase flow. Using the above Eqs. (Eq. (3) to Eq. (8)), the gravity pressure of gas liquid two phase can be obtained by Eq. (9):

$$\left.\begin{aligned} P_3 - P_2 &= (z_2 - z_3)\rho_g g \\ P_1 - P_3 &= (z_3 - z_1)\rho_l g \\ z_1 &= 0 \end{aligned}\right\} \tag{9}$$

Where ρ_g and ρ_l are the density of gas and liquid phase, respectively.

Setting the height of gas layer is h_g, the radius of the pipe is R, then the gravity pressure can be obtained as:

$$\Delta P = P_1 - P_2 = (z_2 - z_3)\rho_g g + (z_3 - z_1)\rho_l g = (h_g\rho_g + (2R - h_g)\rho_l)g \tag{10}$$

Eq. (10) shows that the pressure in the vertical direction is the gravity pressure drop of gas-liquid two-phase flow when the interphase force is not considered. The gravity pressure drop is related to the height of the gas layer, liquid layer and the density of the two phase. The height of gas liquid two-phase in the pipe actually reflects the section area of the two phase, so the gravity pressure is directly related to the void fraction.

The equation of gravity pressure drop can be obtained from the momentum equation of the stratified flow model:

$$\Delta P_{Gr} = \int_0^h \rho_0 g \sin\theta dz = \int_0^h \left[\rho_w \alpha_w + \rho_g \alpha_g\right] g \sin\theta dz \tag{11}$$

Where $\rho_0 g \sin\theta$ is the pressure drop gradient; ρ_w, ρ_g is the density of water and gas; α_w, α_g is the section phase holdups of water and gas; h is the diameter of pipe, g is gravitational acceleration.

For the adiabatic horizontal pipeline, θ=90°, the real gravity pressure drop can be calculated by Eq. (12):

$$\Delta P_{Gr} = (\rho_w \alpha_w + \rho_g \alpha_g)gh \tag{12}$$

The gravity pressure drop perpendicular to the horizontal flow is different from the friction pressure drop, accelerate pressure drop and the gravity pressure drop alongside with a horizontal pipe. It just includes gravity and interphase force, and this can be demonstrated by Eq. (13):

$$\Delta P_v = \Delta P_{Gr} - \Delta P_b \tag{13}$$

Where ΔP_V is the measured pressure drop perpendicular to the horizontal flow, ΔP_{Gr} is the real gravity pressure drop, ΔP_b is the interphase force. The schematic diagram of pressure drop measurement scheme is shown in Fig. 4.

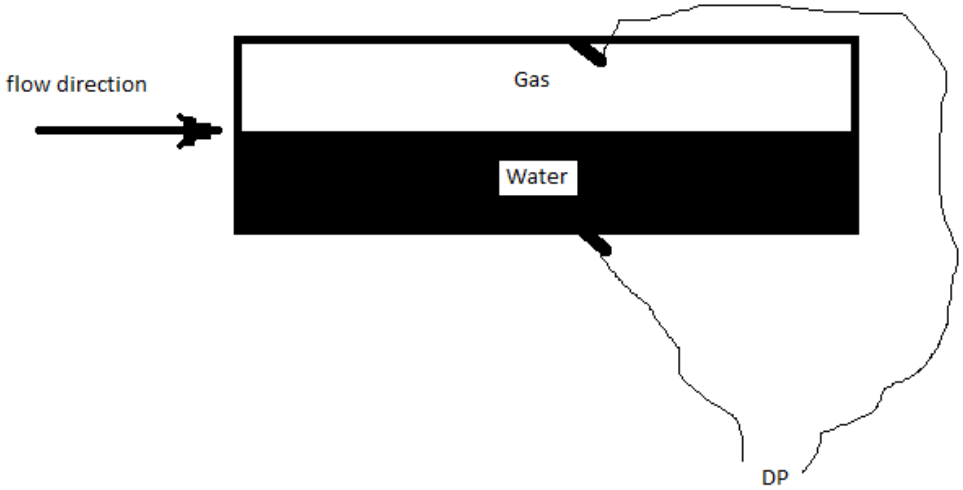

Fig. 4. Schematic diagram of pressure drop measurement scheme.

The interphase force we are studying is per unit area, it can be expressed by pressure. Therefore, the unit of the interphase force is expressed in Pa. And the interphase force can be calculated by Eq. (14)

$$\Delta P_b = \Delta P_{Gr} - \Delta P_v \tag{14}$$

The block diagram of measurement analaysis is shown in Fig. 5. The interphase forces can be acquired by the following steps：

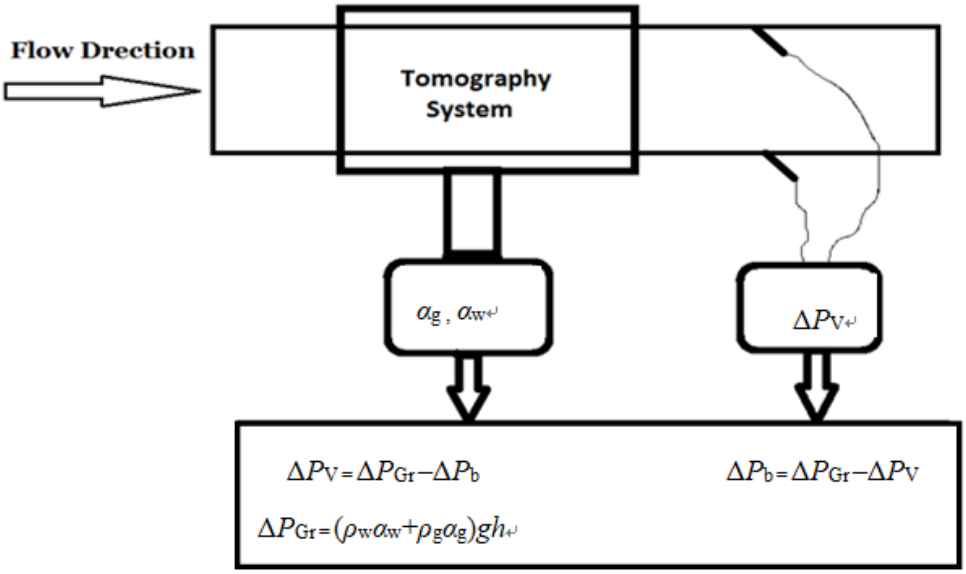

Fig. 5. Block diagram of measurement analaysis.

1) The phase holdups α_w, α_g can be obtained by used the ERT system, then the real gravity pressure drop P_{Gr} can be calculated by Eq. (12);

2) The pressure drop ΔPv perpendicular to the horizontal flow can be obtained by DP sensor;

3) The interphase forces can be acquired by the dual-modality measurement system Eq. (14).

3. Experiment system

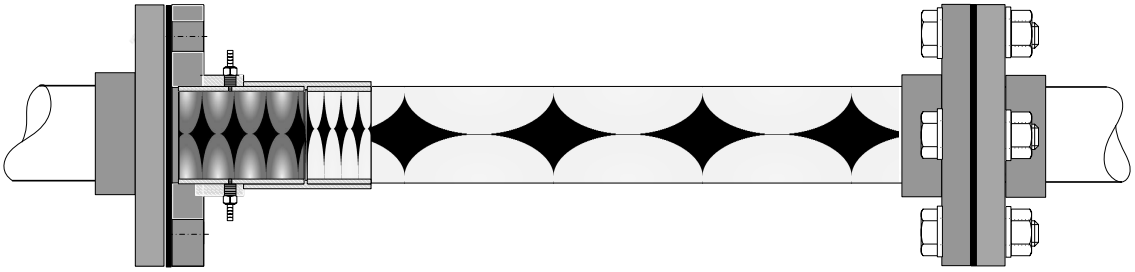

Fig. 6. Air/water horizontal test section including DP measurement points.

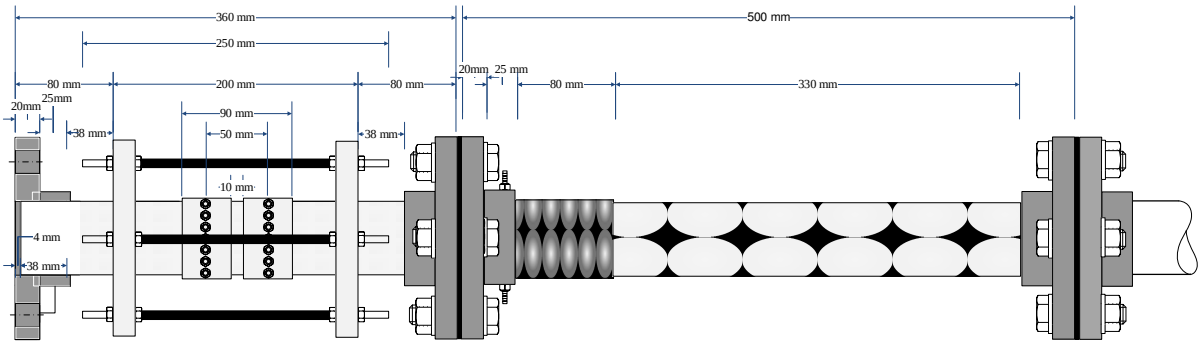

Fig. 7. Air/water horizontal test section including the ERT sensor.

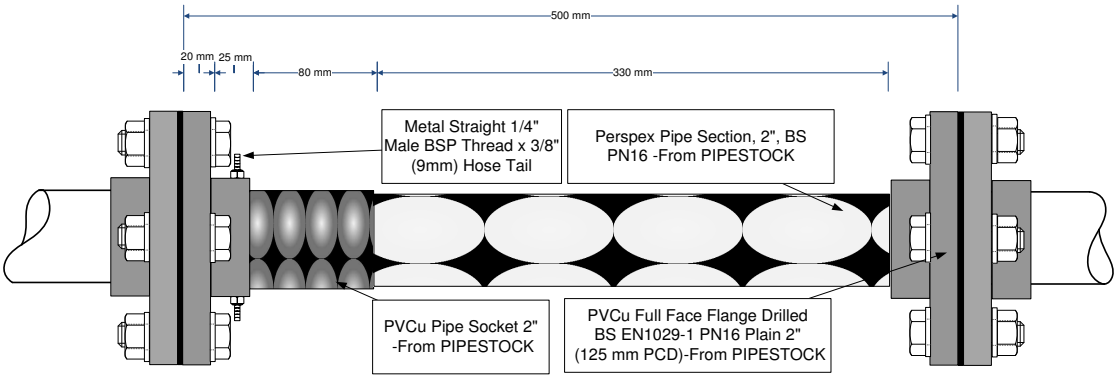

Fig. 8. Air/water horizontal test section with BSP threaded mounted.

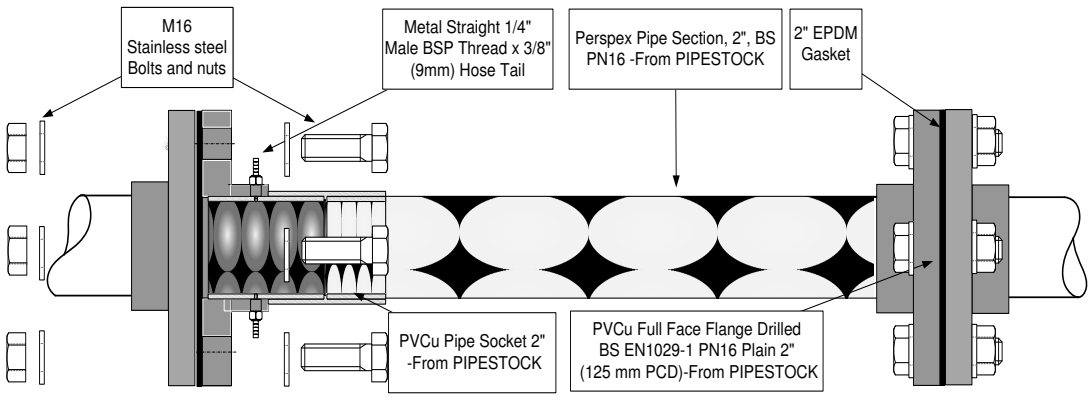

Fig. 9. Air/water horizontal test section and its mechanical components.

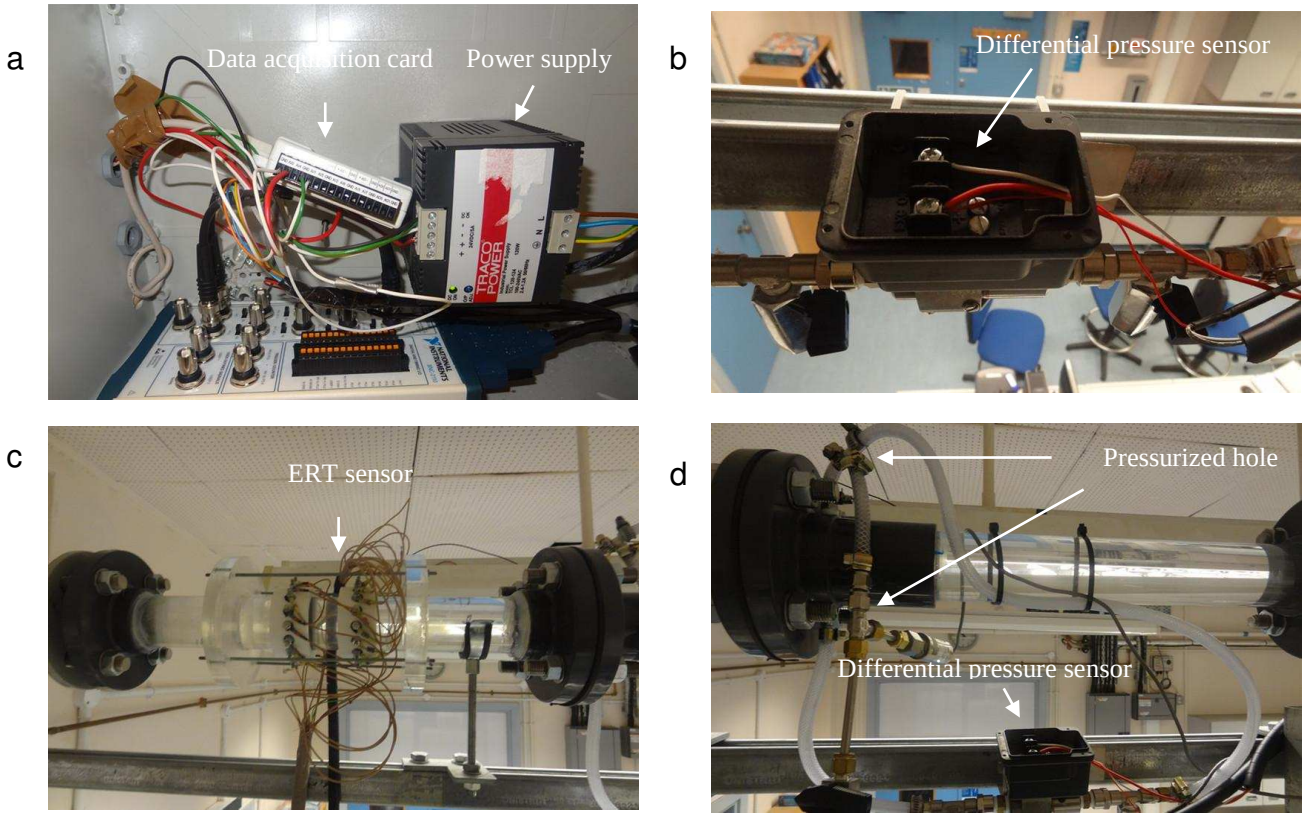

Fig. 10. Experimental system structure of (a) NI data acquisition, (b) Differential pressure sensor, (c) Dual-plane ERT sensor, (d) Test system.

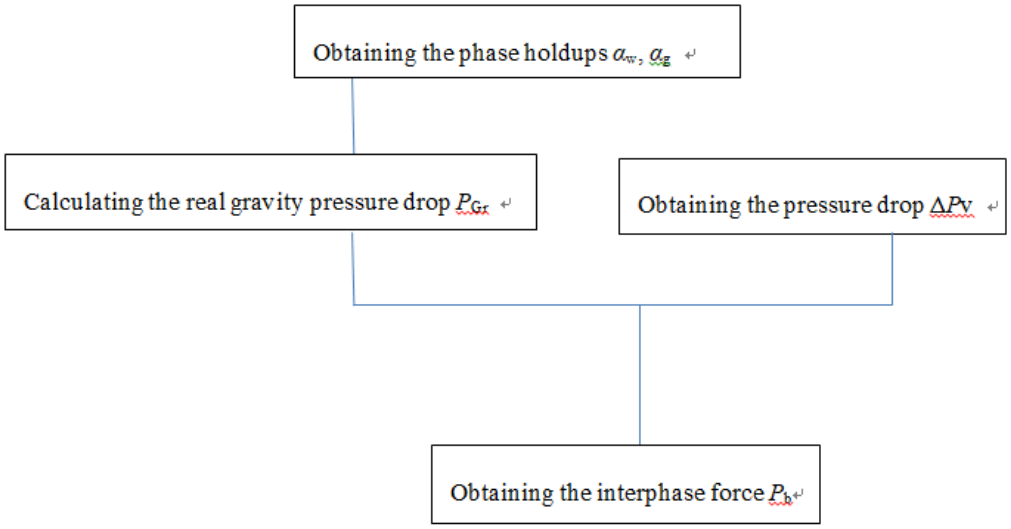

Fig. 11. Flow chart for solving interphase forces.

The interphase forces is the driving force of the evolution of the flow pattern. It is one of the key parameters to reveal the gas-liquid two-phase flow mechanism. The main content of the research is to design a device for quantitative detection of interphase forces of gas-liquid two-phase flow. After theoretical analysis, the theoretical model of the interphase forces was established. The phase holdup is one of the basic parameters of the two-phase flow, and the differential pressure signal perpendicular to the horizontal flow direction can reflect the interaction between the gas-liquid two phases. In this study, the experimental characteristics of the device, including the differential pressure characteristics of the device,

the phase holdup and the interphase force, were comprehensively studied. The experiment was carried out in the horizontal pipe gas-liquid two-phase flow loop at University of Leeds. In horizontal experiment, a test system was designed. Fig. 6-9 show the schematic diagram and photos of the experimental facility. Fig. 10 and Fig. 11 show the experimental system and the flow chart for calculating the interphase forces.

ERT has proven its efficiency to image and monitor spatial phenomena [48]. Professor Williams R.A. and Professor M. Wang of the University of Leeds developed the ERT system and the corresponding patent. In 2001, the new principle of ERT hardware system was developed, which was based on bipolar pulse current source. This technology can overcome the electric polarization effect caused by the conventional direct current excitation source, and the operating speed of the system is faster, which provides a new way to solve the real-time performance [49]. In 2003, the University of Leeds developed a high performance electrical impedance tomography (EIT) system, and used the digital signal processor (DSP, it is a microprocessor suitable for compute dense data operation and real-time signal processing) as the processor, for which data sampling rate reached 1000 samples per second. The repeatability and stability of this system are less than 0.5% and 0.6% respectively. This study employs the ERT system, which was mounted on the gas-water flow facility at the University of Leeds, for measurement of void fraction. The void fraction obtained through electrical conductivity.

The average resistivity across the measurement plane is calculated by averaging the voltage measurements and dividing by the injection current. An ERT system produces a cross-sectional image showing the distribution of electrical conductivity, the system injects a current between a pair of electrodes and measures the resultant voltage difference between remaining electrode pairs according to a pre-defined measurement protocol. The Data acquisition system for ERT is responsible for obtaining the quantitative data describing the state of the conductivity distribution inside the pipeline. The data must be collected quickly and accurately in order to track small changes of conductivity in real-time thus allowing the image reconstruction algorithm to provide an accurate measurement of the true conductivity distribution. The system has an injection current range of 0 to 75 mA which is divided into 3 broad bands (0-1.5, 1.5-15, 15-75) with 256 step changes possible. Also, to accommodate a wide range of material conductivities and to improve the accuracy for slowly changing processes, a range of injected current frequencies is provided. The system can operate within the frequency range 75 to 153.6 kHz (in 12 steps), its maximum electrode is 128, measuring range - 10 V to +10 V. All online measurements are saved and outputted in an Excel readable CSV file format with the extra time stamp, real and imaginary part by its gain information respectively appended to each set of measurement line. Prior to collecting data it is necessary to take a reference measurement since the system works on the principle of taking measurements and comparing these to a known reference measurement. This reference conductivity can be measured with a conductivity probe prior to taking the reference measurement or can be taken from literature. All subsequent measurements are based on changes in voltage measurements in relation to the reference measurement. Following the collection of a reference measurement, data collection can be initiated before any changes are made to the contents of the sensor. The injection current can be altered to minimize the relative change (noise) between the reference data and subsequent measurement data. In order to overcome the problem associated with various process vessel sizes and differing conductivities of materials it is useful to have the facility to increase or decrease the amplitude of the injected current in order to optimise the signal-to-noise ratio (SNR) of the measured voltage outputs for specific applications. In all cases, the voltage measurements pass through a multiplexer into a differential input amplifier which amplifies the potential difference between the two input voltage signals. The amplifier has the ability to reject common-mode signals such as electrical noise. The sine-wave output of the differential amplifier is

then fed into a programmable gain amplifier (PGA) to accommodate the wide dynamic range of voltage signals obtained from the many pairs of electrodes. A phase-sensitive demodulator (PSD) is employed after the PGA to demodulate the voltage signals prior to low-pass filtering. Fig. 12 shows the tomography results at water flow rate 3.26 m^3/h and the range of gas flow rate 0-3.6 m^3/h. The blue color represents the gas phase at the top of the pipe, while the green color represents the water phase at the bottom of the pipe in the horizontal test section.

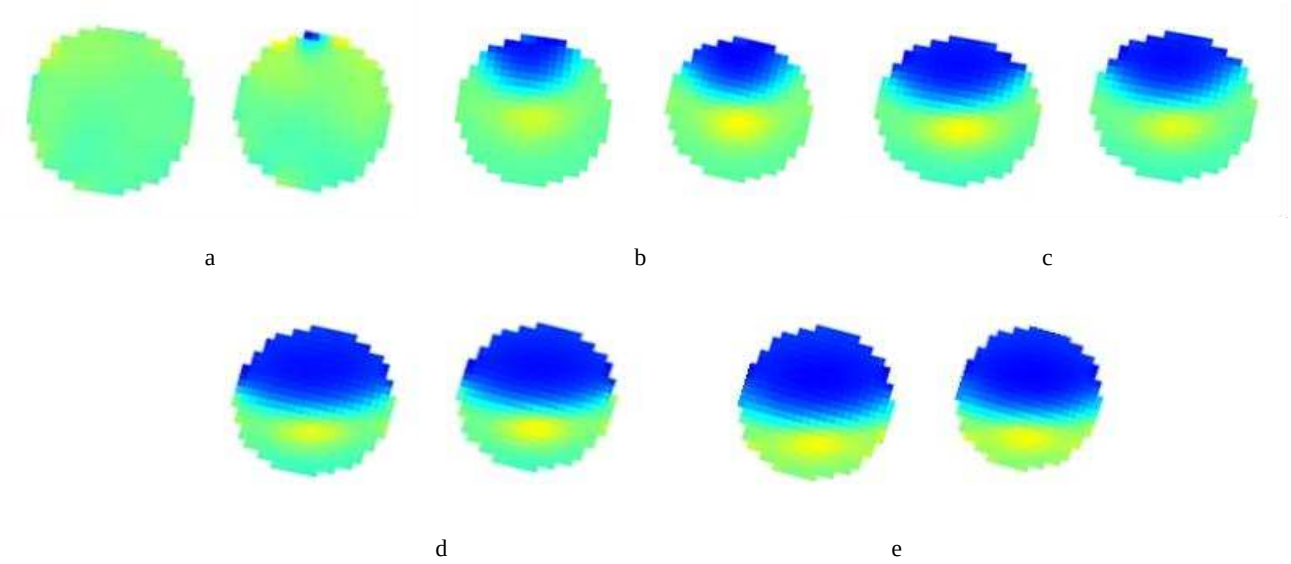

Fig. 12. The tomography results at different gas flow rate in the horizontal pipe section. (a) Gas flow rate 0 m^3/h, (b) Gas flow rate 0.06 m^3/h, (c) Gas flow rate 0.3 m^3/h, (d) Gas flow rate 1.2 m^3/h, and (e) Gas flow rate 3.6 m^3/h.

4. Data analysis

Table 1

Part of data of water flow rate and gas flow rate along with the measured differential pressure at each condition.

Water Flow Rate (rpm)	EMF reading (m^3/h)	Gas Flow Rate (l/min)	Gas Flow Rate (m^3/h)	Differential Pressure (Pa)	Max (Pa)	Min (Pa)
60	3.2577	0	0	2080	2752	1419
60	3.2577	1	0.06	2020	2283	1716
63	3.4059	5	0.3	1997	2943	1173
60	3.2577	20	1.2	1963	4305	-250
65	3.5047	60	3.6	1886	3265	42
102	5.3325	0	0	2054	2741	1412
100	5.2337	1	0.06	2020	2708	1272
100	5.2337	5	0.3	2022	3759	405
100	5.2337	20	1.2	2005	3137	855
100	5.2337	60	3.6	1935	3742	625
143	7.3579	0	0	2091	2672	1529
143	7.3579	1	0.06	2028	2624	1390
143	7.3579	5	0.3	2028	2782	1423
143	7.3579	20	1.2	2022	2855	1287
135	6.9627	60	3.6	1950	3364	760

Three group of water flow rate are selected for the test, and nine group of gas flow rate are implemented in each water flow rate condition. Sampling frequency of experiment is 1 kHz, the test period is 10 second, and 10000 frames were collected for each test condition. A part of data test by the dual-modality measurement system are listed in the Table 1, which shows the input water flow rate and gas flow rate along with the measured differential pressure at each condition.

Fig.13 shows the differential pressure and absolute pressure signals obtained at gas flow rate of 0 m^3/h, and a range of water flow rate 3.26-7.36 m^3/h. There is no interphase force in this case, and the fluctuation of the pressure difference signal is very small.

Fig. 14-16 show the differential pressure and absolute pressure signals obtained at constant water flow rate and different gas flow rate. By observing these figures, it can be seen that differential pressure signals further fluctuates as the gas flow rate increased, the fluctuation range become wider and the absolute pressure signals increases with increase of gas flow rate. It can also be seen that the phenomena of slug flow is represented by periodic high picks along the measured signals, as the slugs pass through the DP sensor.

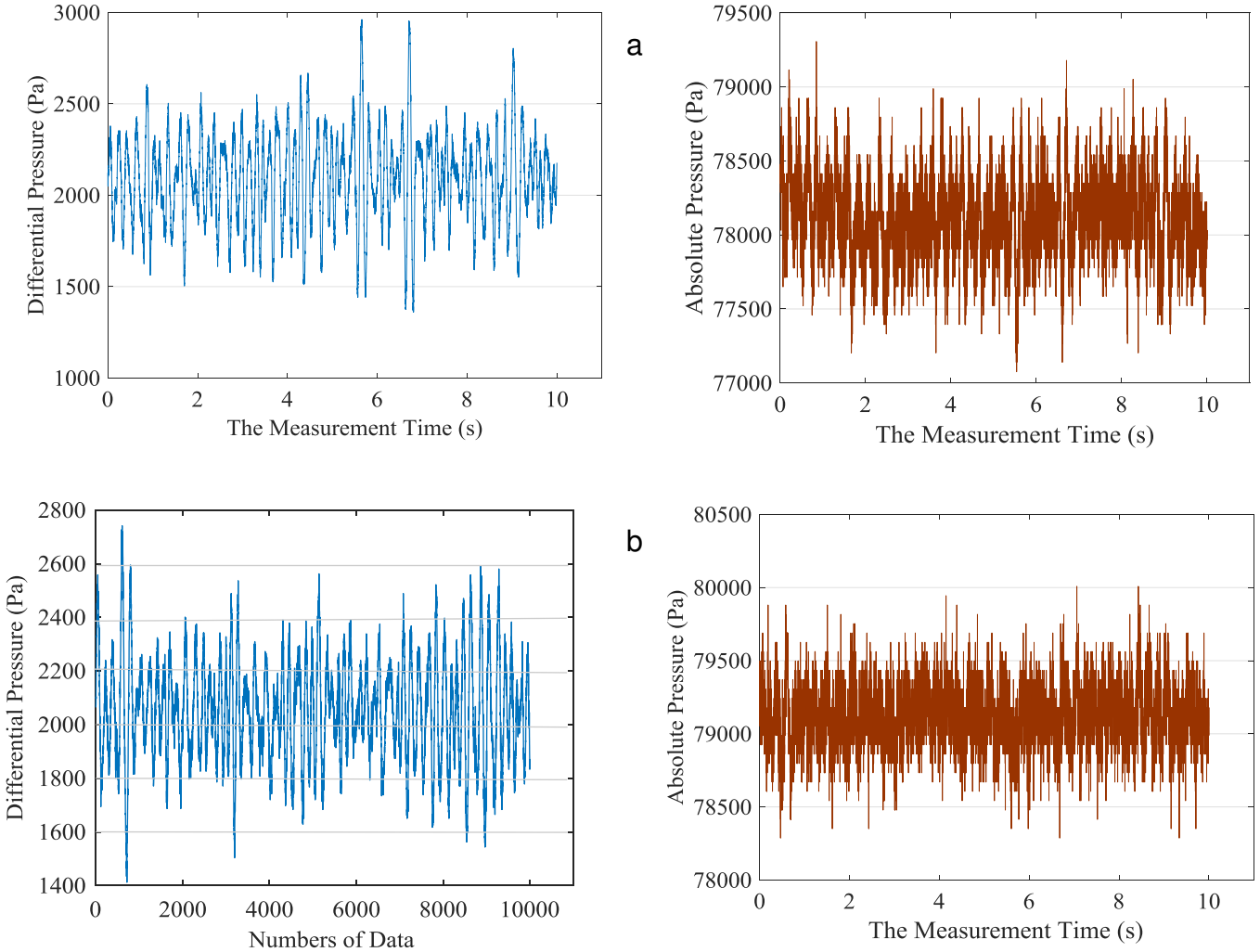

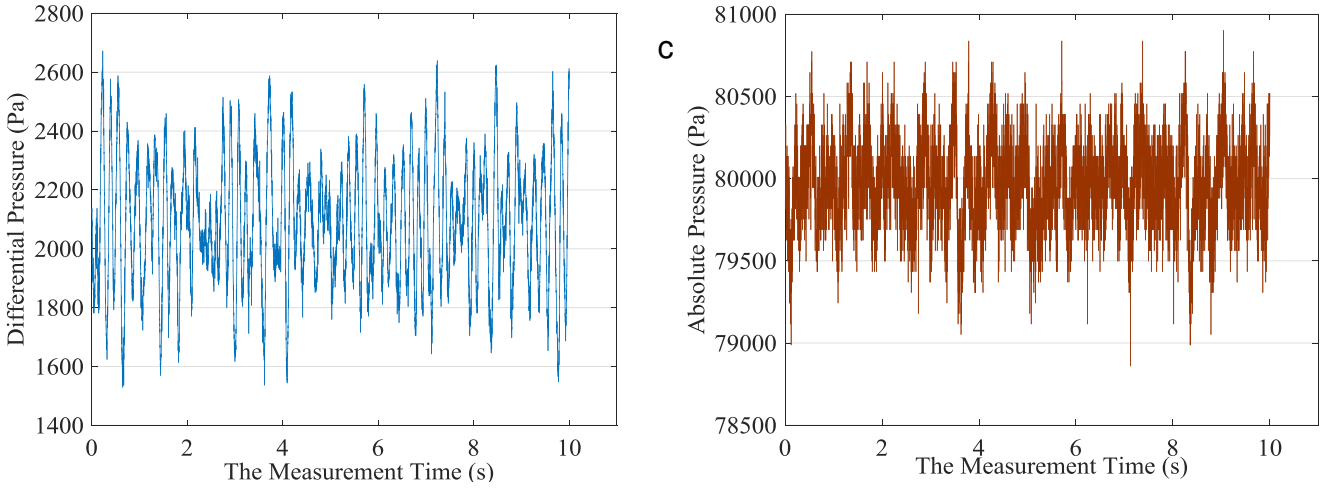

Fig. 13. Differential pressure and absolute pressure signals at gas flow rate of 0 m^3/h and different water flow rate of (a)Water flow rate 3.26 m^3/h, (b)Water flow rate 5.23 m^3/h, (c) Water flow rate 7.36 m^3/h.

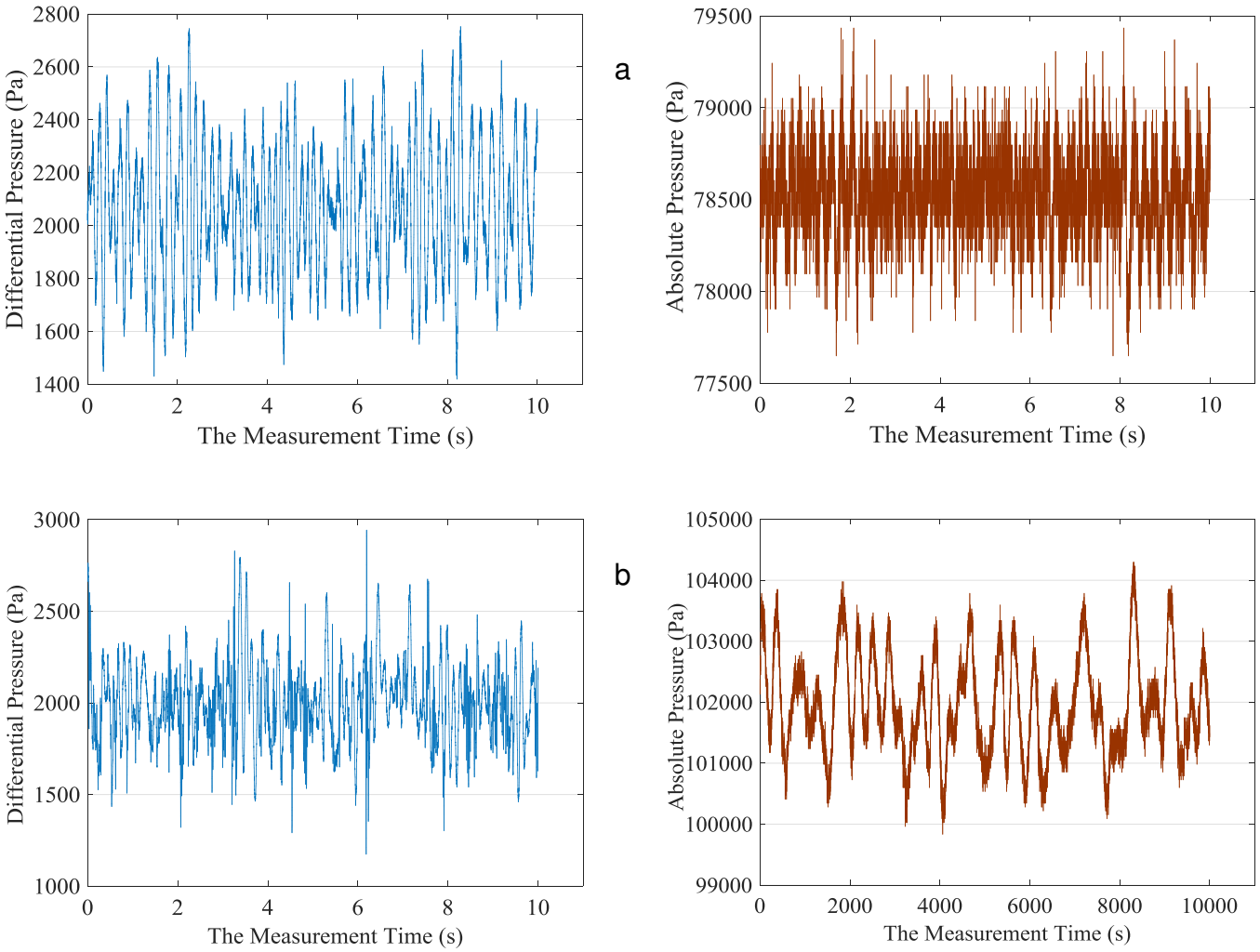

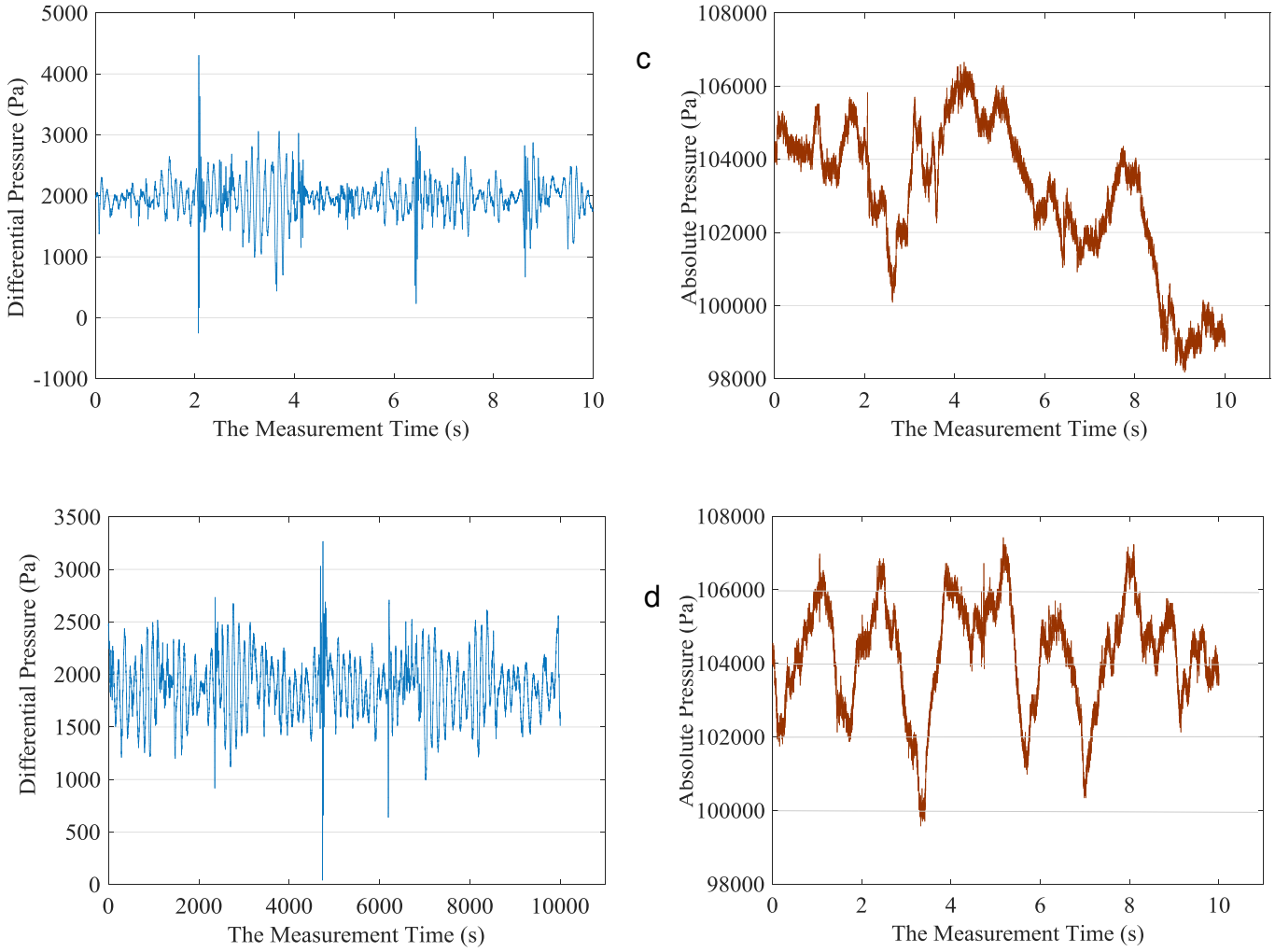

Fig. 14. Differential and absolute pressure signals at water flow rate of 3.26 m^3/h and different gas flow rate of (a) Gas flow rate 0.06 m^3/h, (b) Gas flow rate 0.3 m^3/h, (c) Gas flow rate 1.2 m^3/h, (d) Gas flow rate 3.6 m^3/h.

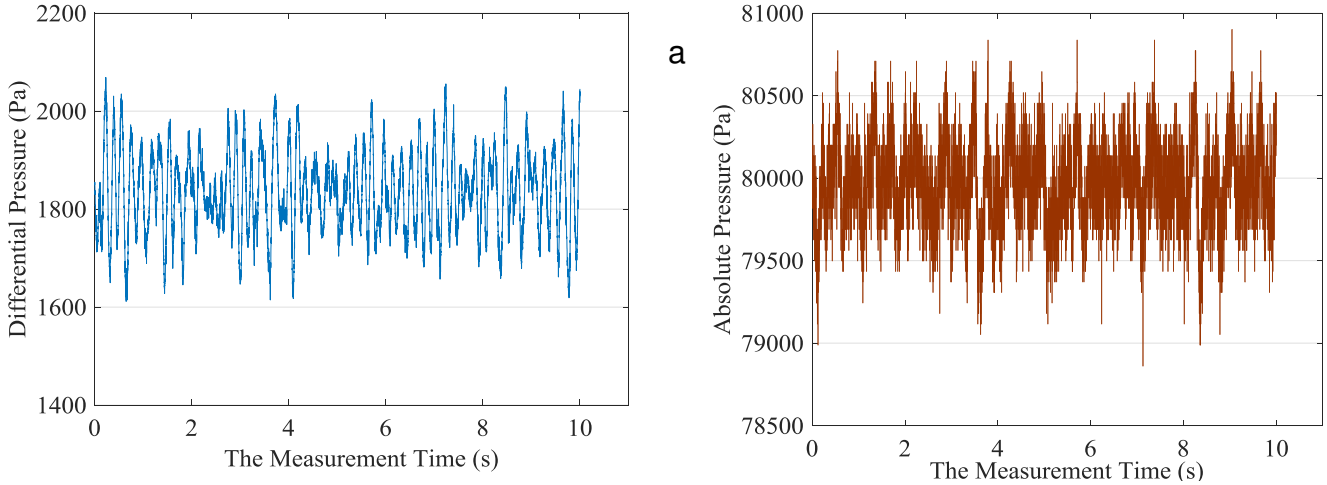

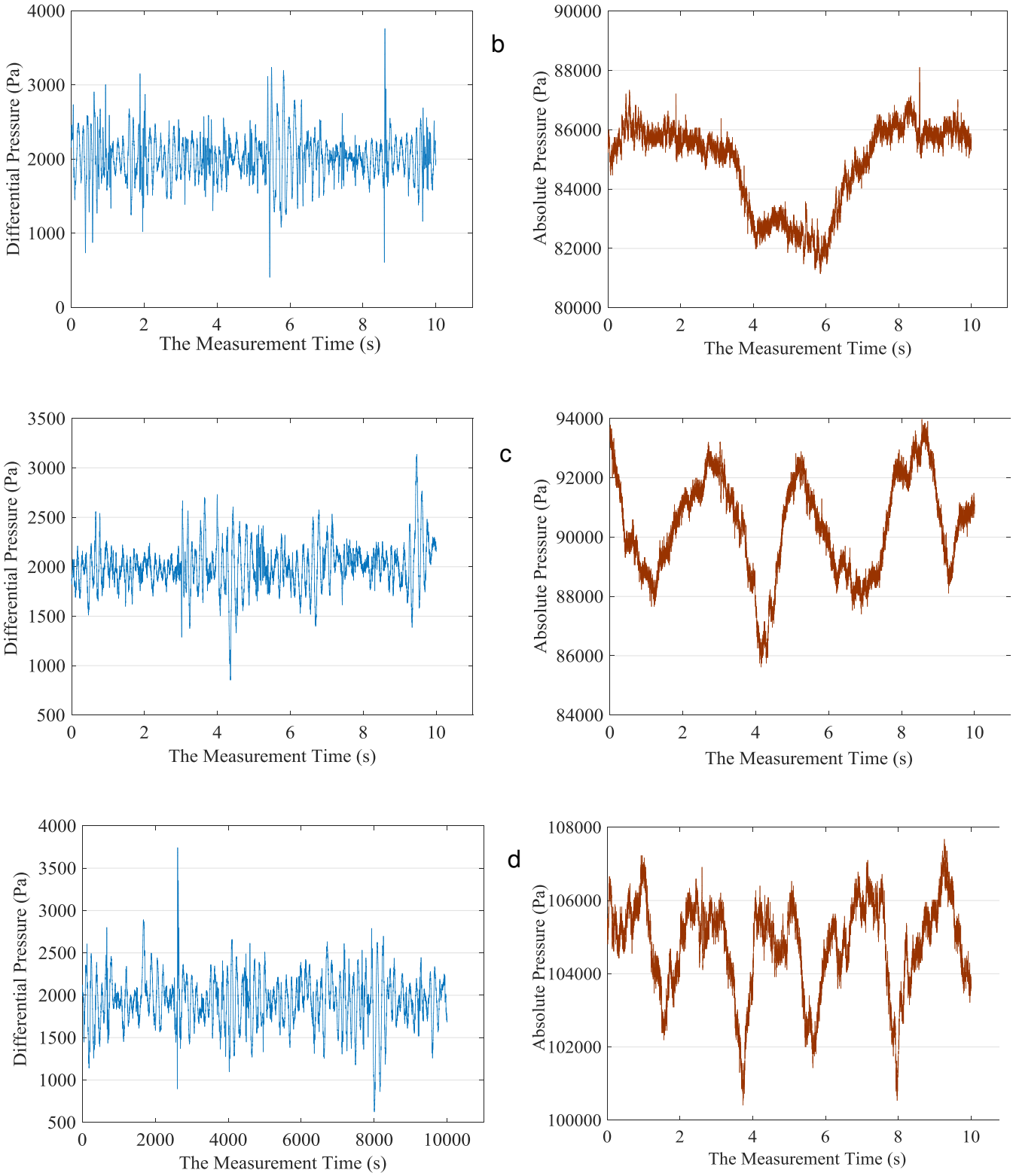

Fig. 15. Differential and absolute pressure signals at water flow rate of 5.23 m^3/h and different gas flow rate of (a) Gas flow rate 0.06 m^3/h, (b) Gas flow rate 0.3 m^3/h, (c) Gas flow rate 1.2 m^3/h, (d) Gas flow rate 3.6 m^3/h.

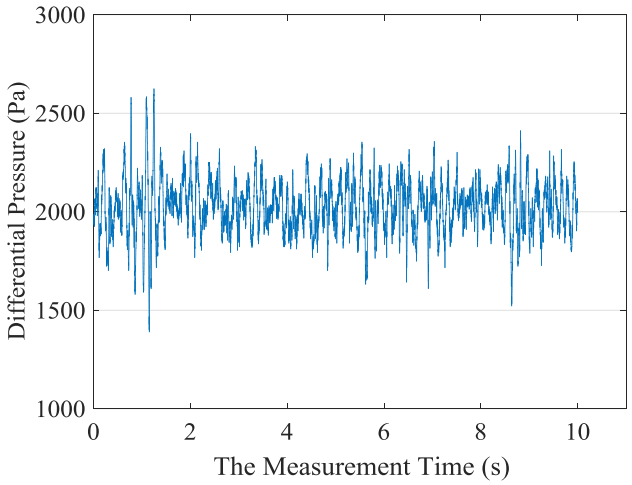
Differential Pressure (Pa)
3000
2500
2000
1500
1000
0
2
4
6
8
10
The Measurement Time (s)

a

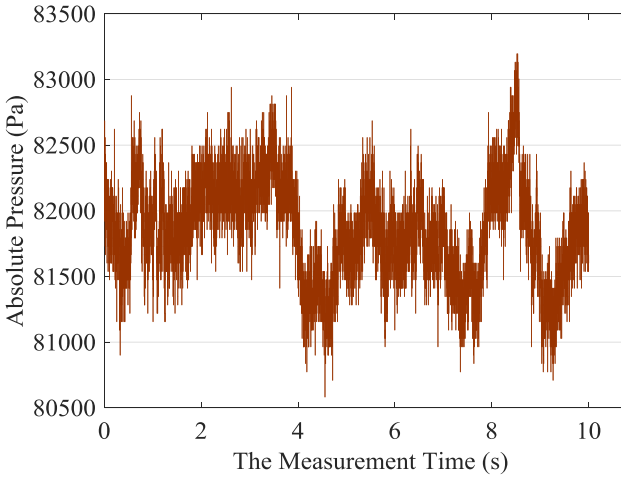
Absolute Pressure (Pa)
83500
83000
82500
82000
81500
81000
80500
0
2
4
6
8
10
The Measurement Time (s)

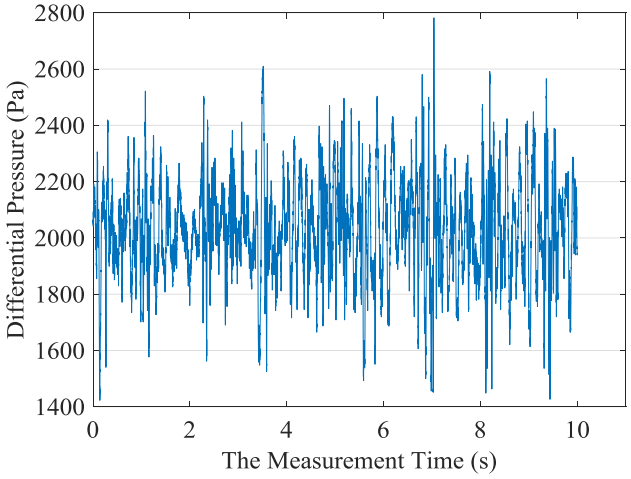
Differential Pressure (Pa)
2800
2600
2400
2200
2000
1800
1600
1400
0
2
4
6
8
10
The Measurement Time (s)

b

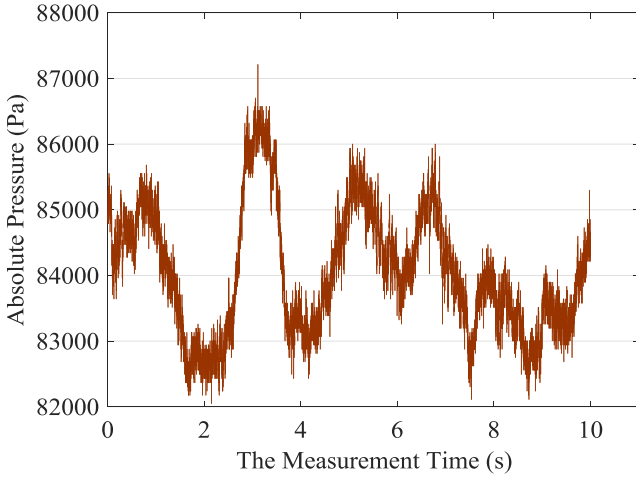
Absolute Pressure (Pa)
88000
87000
86000
85000
84000
83000
82000
0
2
4
6
8
10
The Measurement Time (s)

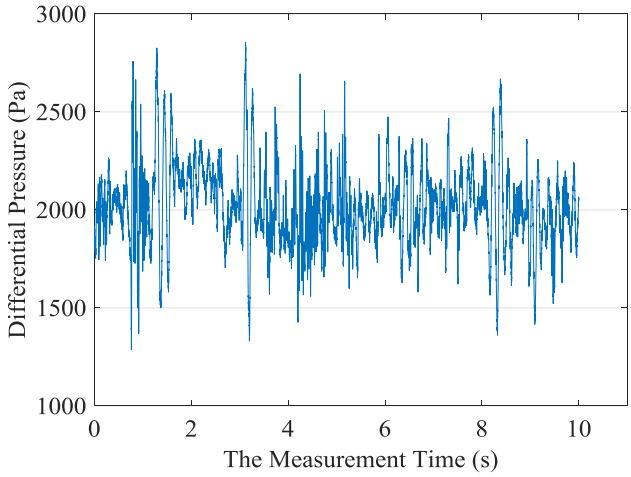
Differential Pressure (Pa)
3000
2500
2000
1500
1000
0
2
4
6
8
10
The Measurement Time (s)

c

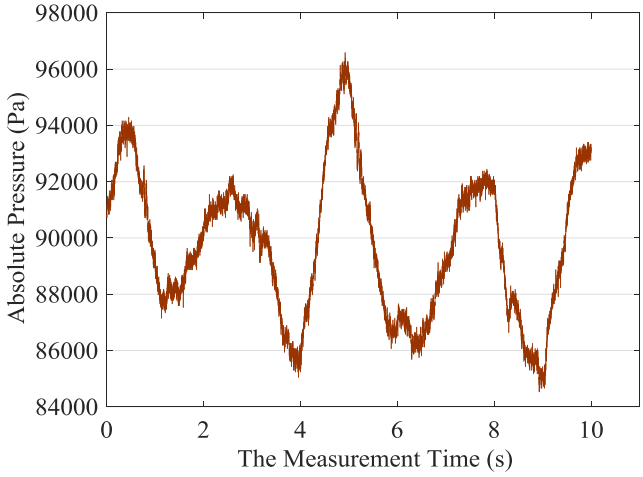
Absolute Pressure (Pa)
98000
96000
94000
92000
90000
88000
86000
84000
0
2
4
6
8
10
The Measurement Time (s)

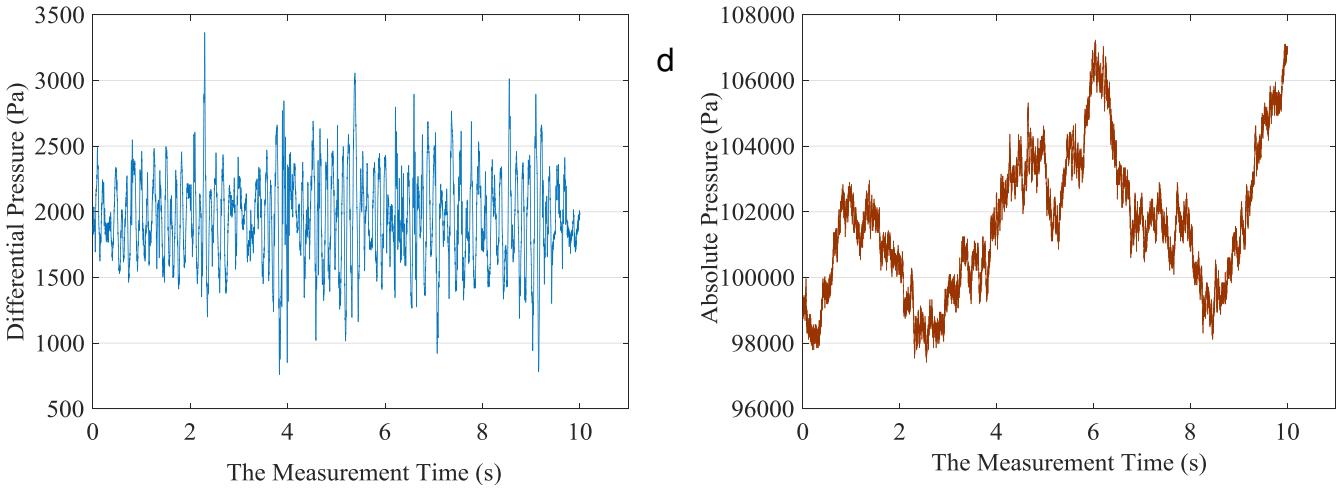

Fig. 16. Differential and absolute pressure signals at water flow rate of 7.36 m^3/h and different gas flow rate of (a) Gas flow rate 0.06 m^3/h, (b) Gas flow rate 0.3 m^3/h, (c) Gas flow rate 1.2 m^3/h, (d) Gas flow rate 3.6 m^3/h.

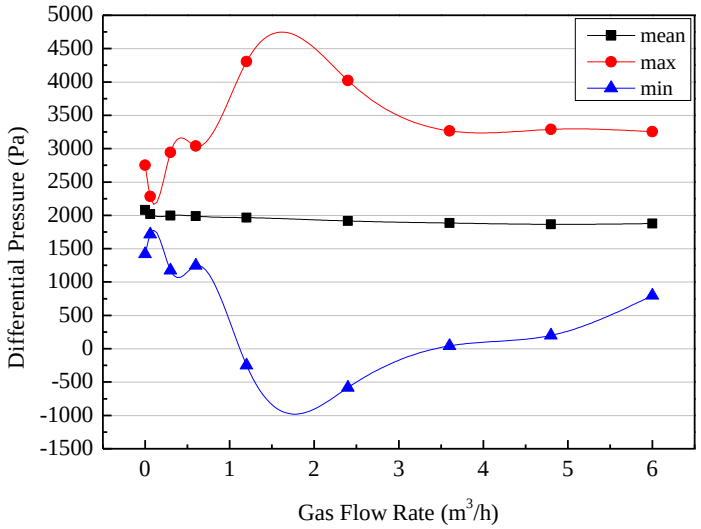

Fig. 17. Differential Pressure drop at water flow rate of 3.26 m^3/h.

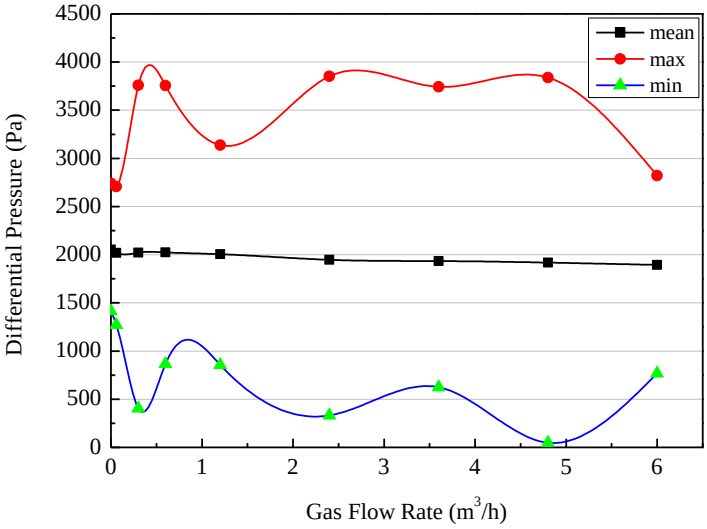

Fig. 18. Differential Pressure drop at water flow rate of 5.23 m^3/h.

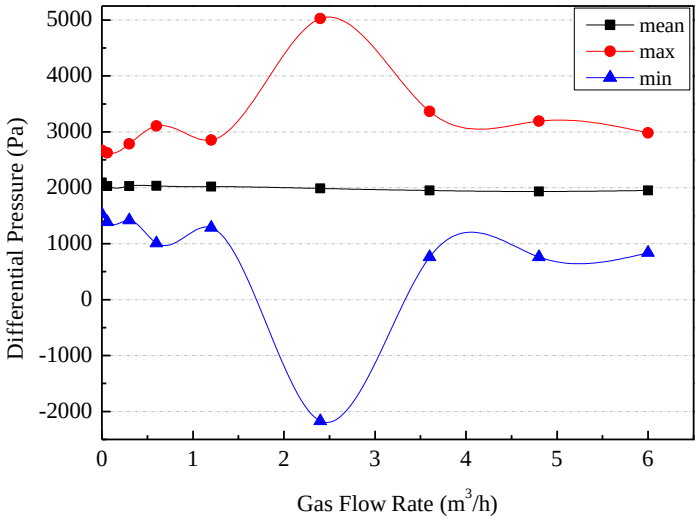

Fig. 19. Differential Pressure at water flow rate of 7.36 m^3/h.

Fig. 17-19 show the average, maximum and minimum differential pressure across the cross-sectional area of the horizontal pipe. It can be seen that the average pressure drop decreases with the increase of gas flow rate. Based on this trend, a correlation can be established.

Fig. 20 shows that the mean differential pressure at water flow rates 3.26 m^3/h, 5.23 m^3/h and 7.36 m^3/h, respectively. At constant gas flow rate, the faster the water flow rate, and the greater the differential pressure can be observed. By increasing of gas flow rate, the entrainment force of gas phase on the liquid phase is increased, and the gravity of the liquid phase decreases. As previously mentioned, the pressure difference perpendicular to the flow direction is mainly caused by the pressure drop of the gravity pressure drawdown, so the differential pressure signal perpendicular to the horizontal flow direction continuously decreases, and the same phenomena is observed at different water flow rates.

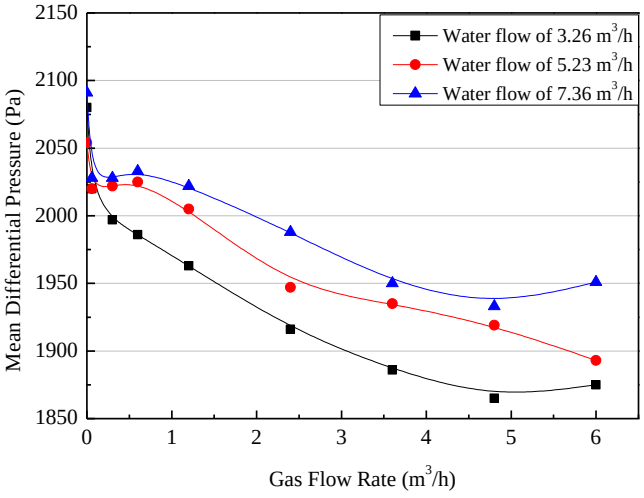

Fig. 20. Mean Differential Pressure at different water flow rate.

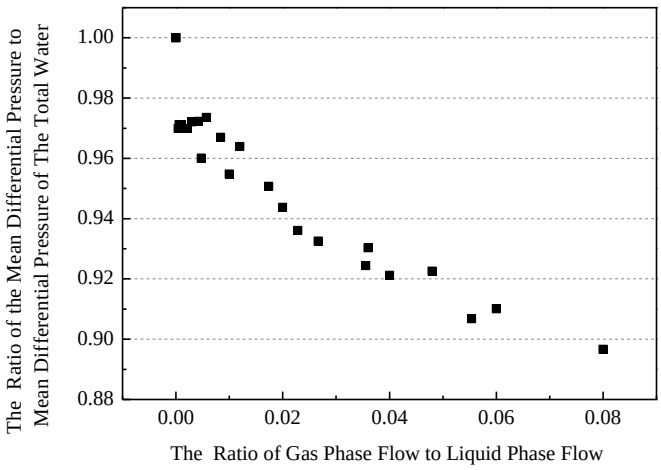

Fig. 21. The relationship of mean differential pressure ratio and flow rate ratio.

Taking the ratio of gas phase flow to liquid phase flow as the x-axis, and the ratio of the mean differential pressure to mean differential pressure of the total water as the y-axis to plot the Fig. 21, it can be seen that there is a certain law between them, the model is shown in Eq. (15).

$$y = -250.0488x^3 + 40.9801x^2 - 2.7847x + 0.9841 \quad (15)$$

The relation between the interphase force and void fraction is shown in Fig. 22. The relation between the interface force and different water flow rates, 3.26 m^3/h, 5.23 m^3/h, 7.36 m^3/h, is shown in Fig. 23. The interphase force is gradually increases as the void fraction increases. This is due to the fact that with increasing void fraction, the entrainment force of gas phase increases and the gravity of the liquid phase decreases. From the aforementioned figures, it is quite apparent that the interface force demonstrate similar trend at different water flow rate. The analysis results show that accurately obtaining the differential pressure perpendicular to the horizontal flow direction is the key to obtain the interface force.

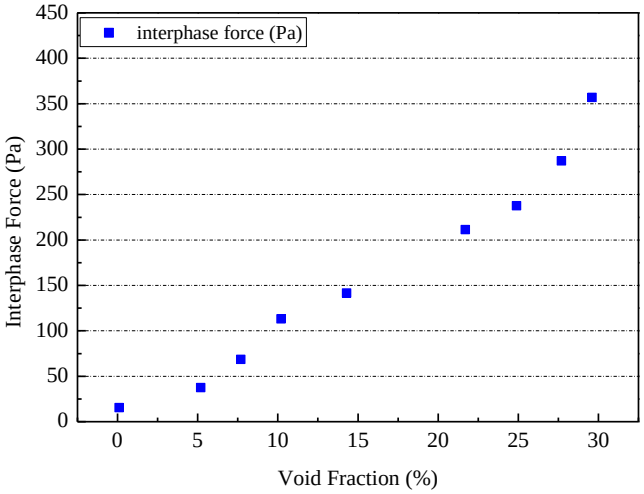

Fig. 22. Relation of interphase force and void fraction.

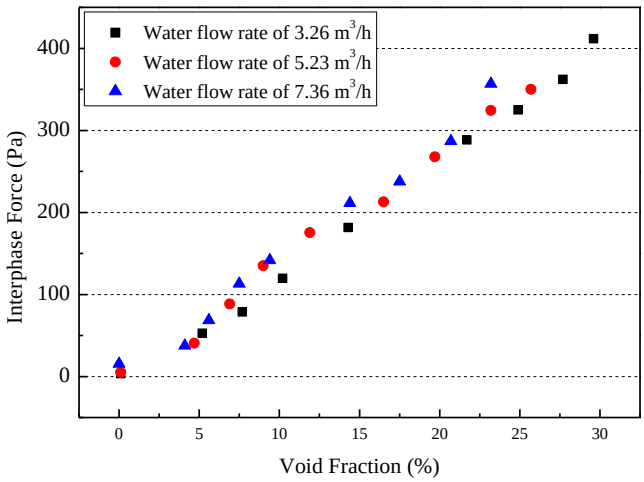

Fig. 23. Relation of interphase force and void fraction.

$$Fr_g = \frac{Jg}{\sqrt{gD}}\sqrt{\frac{\rho_l}{\rho_l - \rho_g}} = \frac{4m_g}{\rho_g \Pi \cdot D^2 \sqrt{gD}}\sqrt{\frac{\rho_l}{\rho_l - \rho_g}} \tag{16}$$

$$Fr_l = \frac{J_l}{\sqrt{gD}}\sqrt{\frac{\rho_l}{\rho_l - \rho_g}} = \frac{4m_l}{\rho_l \Pi \cdot D^2 \sqrt{gD}}\sqrt{\frac{\rho_l}{\rho_l - \rho_g}} \tag{17}$$

Where Fr_l, Fr_g are the Froude Number of liquid phase gas phase; J_g, J_l are the superficial velocity of the gas phase and liquid phase, m/s; g is the acceleration of gravity; m_g, m_l are the gas and liquid mass flow rate, kg/s; D is the pipe diameter, m; ρ_g, ρ_l are the gas phase density and liquid phase density, kg/m^3.

Fr_l and Fr_g contain both flow information and void fraction information. Taking Fr_g as the x-axis, Fr_l as the y-axis, and the interface force as the z-axis, the relationship diagram is plotted in Fig. 24. As shown in Fig. 24, the interface force is closely related to the Fr_g, when Fr_1 is the same, the interphase force increases as the Fr_g increases.The model was established with the water flow rates of 3.26 m^3/h and 5.23 m^3/h and by introduced the Frg, ρ_g and ρ_l. The relationship between the interphase force and void fraction can be summarized by the following Eq. (18).

$$\frac{\Delta P_b}{\overline{\Delta P_0}} = 1.3797 \cdot (F_{rg})^{0.0881} \cdot \left(\frac{\rho_L}{\rho_g}\right)^{0.6006} \cdot \alpha + 0.0091 \cdot (F_{rg})^{0.48366} \cdot \left(\frac{\rho_L}{\rho_g}\right)^{0.46958} \tag{18}$$

Where ΔP_b is interphase force, Pa; $\overline{\Delta P_0}$ is interphase force of the total water, Pa.

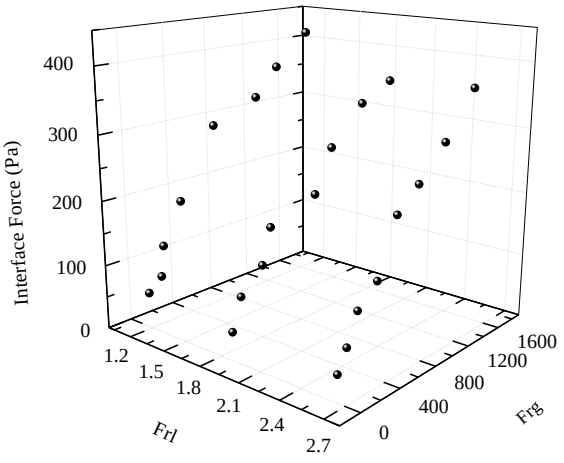

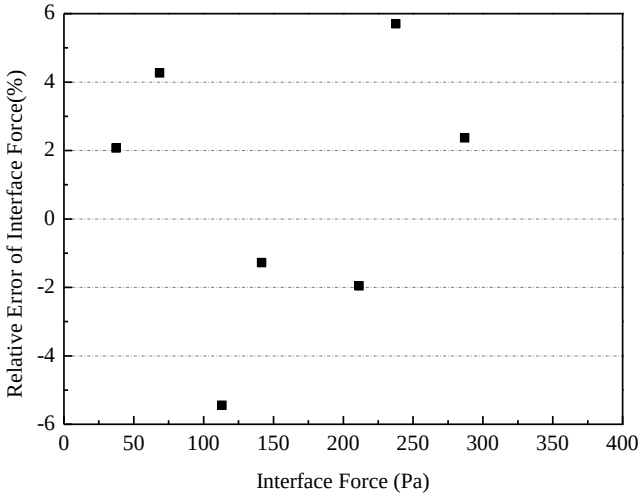

Fig. 24. The relationship of interphase force and Frg, Frl.

Fig. 25. Relative error of interphase force.

The model was tested with the effect of the water flow at 7.36 m^3/h. The ratio of the interface force to the interface force of the total water is obtained, the relative error was obtained by compared with the actual ratio value. As shown in Fig. 25, the relaltive error of the interface force is within ±6 %.

5. Conclusion

In this work, a dual-modality measurement system is developed for evaluation of interphase forces of gas-liquid two phase flow perpendicular to the horizontal flow direction.

Based on the basic equations of gas-liquid two phase flow and the definition of flow parameters, a theoretical model for the interphase force of gas-liquid two-phase flow perpendicular to horizontal direction was developed. It is expected that the developed model to provide a theoretical basis for quantitative calculation of interphase force in horizontal two-phase gas-liquid flow. The obtained results demonstrated that the pressure difference in the vertical direction perpendicular to the horizontal flow direction can be related to the magnitude of the interphase force. An electrical resistance tomography system was used to obtain the void fraction, from which the gravity pressure drop can be obtained. The pressure drop perpendicular to the horizontal flow also can be obtained by DP sensor.

The relationship between the differential pressure drop and inter-phase force was established, the experimental results demonstrated that the interphase force quantitative measurement device was successfully able to provide a quantitative evaluation of interphase forces in two-phase horizontal gas-water flow.

It is worth mentioning that with the development of multiphase flow detection technology, the detection of interphase force will become the key in the study of pressure drop. In order to fully and accurately understand the interphase force, several related issues will be the subject of future investigations,

1) To further improvement of mechanical aspect and design of the device;

2) Due to the limitation of the measurement points and the accuracy of the differential pressure sensor in the experiment, the selection of a higher precision differential pressure sensor can improve the measurement accuracy.

3) When measuring the void fraction of the section, the design or measurement method of the ERT system can further improved, so the measurement accuracy is higher.

4) In the future, the measurement model of the interphase force can be considered for further derivation and improvement.

Acknowledgements

The authors are grateful for the support by the National Natural Science Foundation of China (61475041), Natural Science Foundation of Hebei Province (E2017201142), the Subtask National Key Research Task Plan (2016YFF0203103-3,2017YFC0805703), and Funds Supported by the Hebei Giants Plan (201501).

References

[1] A. Brito, N. Guzmán, L. Rojas-Solórzano, T. Zambrano, Rheological study of two- and three-phase highly viscous fluid flow in pipelines, J. Pet. Sci. Eng. 170 (2018) 772-784.

[2] H. Shahverdi, M. Sohrabi, A mechanistic model for prediction of three-phase flow in petroleum reservoirs, J. Pet. Sci. Eng. 157 (2017) 507-518.

[3] A.K. Thandlam, T.K. Mandal, S.K. Majumder, Flow pattern transition, frictional pressure drop, and holdup of gas non-Newtonian fluid flow in helical tube, ASIAPacific J. Chem. Eng. 10 (2015) 422-437.

[4] F.Raeiszadeh, E. Hajidavalloo, M. Behbahaninejad, P. Hanafizadeh, Modeling and simulation of downward vertical two-phase flow with pipe rotation, Chem. Eng. Res. Des. 137 (2018) 10-19.

[5] N. Falcone, A. Bersano, C. Bertani, M. De Salve, B. Panella, Characterization of water-air dispersed two phase flow, Energy Proced. 126 (2017) 66-73.

[6] S. Ghorai, K.D.P. Nigam, CFD modeling of flow profiles and interfacial phenomena in two-phase flow in pipes, Chem. Eng. Process. 45 (2006) 55-65.

[7] P. Pei, K. Zhang, D.S. Wen, Comparative analysis of CFD models for jetting fluidized beds: The effect of inter-phase drag force, Powder Technol. 221 (2012) 114-122.

[8] J.Y. Feng, I.A. Bolotnov, Interfacial force study on a single bubble in laminar and turbulent flows, Nucl. Eng. Des. 313 (2017) 345-360.

[9] F.C. Liang, Y. Sun, Z.J. Fang, S.T. Sun, Application of multi-slot sampling method for gas-liquid two-phase flow rate measurement, Exp. Therm Fluid Sci. 79 (2016) 213-221.

[10] Q. Wang, W. Yao, Computation and validation of the interphase force models for bubbly flow, Int. J. Heat Mass Transf. 98 (2016) 799-813.

[11] M. Gadiraju, J.P. Jr, S.S. Munukutla, Exact solutions for two phase vertical pipe flow, Mech. Res. Commun. 19 (1992) 7-13.

[12] M.V. Tabib, S.A. Roy, J.B. Joshi, CFD simulation of bubble column-An analysis of interphase forces and turbulence models, Chem. Eng. J. 139 (2008) 589-614.

[13] Z. Li, J. Wei, B. Yu, Analysis of interphase forces and investigation of their effect on particle transverse motion in particle-laden channel turbulence, Int. J. Multiph. Flow. 88 (2017) 11-29.

[14] D. Rybaczek, M. Kowalewicz-Kulbat, Premature chromosome condensation induced by caffeine, 2-aminopurine, staurosporine and sodium metavanadate in S-phase arrested HeLa cells is associated with a decrease in Chk1 phosphorylation, formation of phospho-H2AX and minor cytoskeletal rearrangements, Histochem. Chem. Cell. Blol. 135 (2011) 263-280.

[15] L. Riaño, L. Belec, J.F. Chailan, Y. Joliff, Effect of interphase region on the elastic behavior of unidirectional glass-fiber/epoxy composites, Compos. Struct. 198 (2018) 109-116.

[16] R. Liu, B. Yang, E. Zio, X. Chen, Artificial intelligence for fault diagnosis of rotating machinery: A review, Mech. Syst. Signal Proc. 108 (2018) 33-47.

[17] N. Ahmadi, G. Akbarizadeh, Hybrid robust iris recognition approach using iris image pre-processing, two-dimensional gabor features and multi-layer perceptron neural network/PSO, IET Biom. 7 (2018) 153-162.

[18] G. Akbarizadeh, A new statistical-based kurtosis wavelet energy feature for texture recognition of sar Images, IEEE Trans. Geosci. Remote. 50 (2012) 4358-4368.
[19] M. Modava, G. Akbarizadeh, A level set based method for coastline detection of SAR Images, ICPR (2017).
[20] M. Liu, Y. Wu, P. Zhang, Q. Zhang, Y. Li, M. Li, Sar target configuration recognition using locality preserving property and Gaussian mixture distribution, IEEE Geosci. Remote Sens. Lett. 10 (2013) 268-272.
[21] G. Liu, L. Jiao, F. Liu, H. Zhong, S. Wang, A new patch based change detector for polarimetric sar data, Pattern Recognit. 48 (2015) 685-695.
[22] H. Ramezani, H. Zakidizaji, H. Masoudi, G. Akbarizadeh, A new DSWTS algorithm for real-time pedestrian detection in autonomous agricultural tractors as a computer vision system, Measurement 93 (2016) 126-134.
[23] A. Alzeyadi, T. Yu, Moisture determination of concrete panel using SAR imaging and the K-R-I transform, Constr. Build. Mater. 184 (2018) 351-360.
[24] G. Akbarizadeh, M. Rahmani, A new ensemble clustering method for PolSAR image segmentation, Information and Knowledge Technology IEEE. (2015) 1-4.
[25] D. Karimi , G. Akbarizadeh, K. Rangzan, M. Kabolizadeh, Effective supervised multiple-feature learning for fused radar and optical data classification, IET Radar Sonar Navig. 11 (2017) 768-777.
[26] A.Venugopal, A. Agrawal, S.V. Prabhu, Performance evaluation of piezoelectric and differential pressure sensor for vortex flowmeters, Measurement 50 (2014) 10-18.
[27] W. Wang, X. Liang, M. Zhang, Measurment of gas-liquid two-phase slug flow with a Venturi meter based on blind source separation, Chin. J. Chem. Eng. 23 (2015) 1447-1452.
[28] H.J. Zhang, W.T. Yue, L.B. Ma, H.L. Zhou, Relationship between fluctuating differential pressure and void fraction of gas-liquid two-phase flow in Venturi tube, J. Chem. Ind. Eng. (China) 56 (2005) 2102-2107 .
[29] S.R.V. Campos, J.L. Baliño, I. Slobodcicov, D.F. Filho, E.F. Paz, Orifice plate meter field performance: Formulation and validation in multiphase flow conditions, Exp. Therm. Fluid Sci. 58 (2014) 93-104.
[30] M.O. Elobeid, L.M. Alhems, A. Al-Sarkhi, A. Ahmad, S.M. Shaahid, M. Basha, J.J. Xiao, R. Lastra, C.E. Ejimb, Effect of inclination and water cut on venturi pressure drop measurements for oil-water flow experiments, J. Pet. Sci. Eng. 147 (2016) 636-646.
[31] F. Liang, Y. Sun, Z .J. Fang, S.T. Sun, Application of multi-slot sampling method for gas-liquid two-phase flow rate measurement, Exp. Therm Fluid Sci. 79 (2016) 213-221.
[32] A. Pal, B. Vasuki, Void fraction measurement using concave capacitor based sensor-Analytical and experimental evaluation, Measurement 124 (2018) 81-90.
[33] S.K. Min, A.L. Bo, W.Y. Won, Y.G. Lee, W.J. Dong, S. Kim, An improved electrical-conductance sensor for void-fraction measurement in a horizontal pipe, Nucl. Eng. Technol. 47 (2015) 804-813.
[34] S. Gabriel, T. Schulenberg, G. Albrecht, W. Heiler, A. Miassoedov, F. Kaiser, T. Wetzel, Optical void measurement method for stratified wavy two phase flows, Exp. Therm. Fluid Sci. 97 (2018) 341-350.
[35] F.R.M. Yunus, R.A. Rahim, S.R. AW, N.M.N. Ayob, C.L. Goh, M.J. Pusppanathan, Simulation study of electrode size in air-bubble detection for dual-mode integrated electrical resistance and ultrasonic transmission tomography, Powder Technol. 256 (2014) 224-332.
[36] G. Annamalai, S. Pirouzpanah, S.R. Gudigopuram, G.L. Morrison, Characterization of flow

homogeneity downstream of a slotted orifice plate in a two-phase flow using electrical resistance tomography, Flow Meas. Instrum. 50 (2016) 209-215.
[37] O. Adetunji, R. Rawatlal, Estimation of bubble column hydrodynamics: Image-based measurement method, Flow Meas. Instrum. 53 (2017) 4-17.
[38] N. Raeisi, A. M. Meymand, G. Akbarizadeh, Scour Depth Prediction in Sand Beds using Artificial Neural Networks and ANFIS Methods, Indian J. Sci.Technol. 8 (2015).
[39] G. Akbarizadeh, Z. Tirandaz, M. Kooshesh, A new curvelet-based texture classification approach for land cover recognition of sar satellite images, Malayas. J. Comput. Sci. 27 (2014) 218-239.
[40] Z. Tirandaz, G. Akbarizadeh, A Two-Phase Algorithm Based on Kurtosis Curvelet Energy and Unsupervised Spectral Regression for Segmentation of SAR Images, IEEE J. Sel. Top. Appl. Earth Observ. 9 (2016) 1244-1264.
[41] G. Akbarizadeh, Z. Tirandaz, Segmentation parameter estimation algorithm Based on curvelet transform coefficients energy for feature extraction and texture description of SAR images, Inf. Knowl. Technol. IEEE. (2015) 1-4.
[42] M. Farbod, G. Akbarizadeh, A. Kosarian, K. Rangzan, Optimized fuzzy cellular automata for synthetic aperture radar image edge detection, J. Electron. Imaging 27 (2018) 1.
[43] L. Fang, Y. liang, Q. Lu, X. Li, R. Liu, X. Wang, Flow noise characterization of gas-liquid two-phase flow based on acoustic emission, Measurement 46 (2013) 3887-3897.
[44] F. Z. Eishita, K. G. Stanley, The impact on player experience in augmented reality outdoor games of different noise models, Entertainment Comput. 27 (2018) 137-149.
[45] L.D. Fang, R. Liu, Q.H. Lu, X.J. Wang, Y.J. Liang, The flow pattern transition identification and interphase force detection of gas-liquid two-phase flow, AASRI Procedia. 3 (2012) 534-539.
[46] T. Haktanir, M. Ardiçlioğlu, Numerical modeling of Darcy-Weisbach friction factor and branching pipes problem, Advances in Engineering Software, Adv.Eng.Softw. 35 (2004) 773-779.
[47] Y. Liao, X. Li, W. Zhong, G. Tao, Study of pressure drop-flow rate and flow resistance characteristics of heated porous materials under local thermal non-equilibrium conditions, Int.J.Heat and Mass Transfer. 102 (2016) 528-543.
[48] T. Hermans, S. Wildemeersch, P. Jamin, P. Orban, S. Brouyère, A. Dassargues, F. Nguyen, Quantitative temperature monitoring of a heat tracing experiment using cross-borehole ERT, Geoterm. 53 (2015) 14-26.
[49] J. Jia, M. Wang, H.I. Schlaberg, H. Li, A novel tomographic sensing system for high electrically conductive multiphase flow measurement, Flow Meas. & Instru. 21 (2010) 184-190.

Highlights

- Theoretical model for interphase force in gas-water two-phase flow was established
- Effects of differential pressure and void fraction on interphase force was analyzed
- Developed a dual-modality system to measure differential pressure and void fraction
- The system was used to provide a quantitative evaluation of interphase forces